J. Mech. Phys. Solids Vol. 31, No. 5, pp. 405–426, 1983.
Printed in Great Britain.

0022–5096/83 $3.00 + 0.00
Pergamon Press Ltd.

NECK PROPAGATION

J. W. HUTCHINSON

Division of Applied Sciences, Harvard University, Cambridge, MA 02138, U.S.A.

and

K. W. NEALE

Department of Civil Engineering, University of Sherbrooke, Sherbrooke, Quebec, Canada

(*Received* 25 *March* 1983)

ABSTRACT

PROPAGATION of a neck along the length of a tensile specimen as occurs in certain polymeric materials and in a few metals is studied. Two material models are considered: a nonlinear elastic solid, and an inelastic flow theory solid with both rate-dependent and rate-independent behaviors. For the elastic solid the states ahead and behind the neck transition can be obtained fairly simply from just the jump conditions governing continuity of mass, momentum and energy. For the inelastic solid a full three-dimensional analysis must be performed to obtain the same information, and an analysis of axisymmetric neck propagation is carried out.

1. INTRODUCTION

NECKING in a tensile test sets in if the uniaxial nominal (engineering) stress–strain curve of the specimen material has a maximum. For metals whose uniaxial nominal curve peaks and then falls monotonically, a neck forms at some section of the tensile specimen and remains localized with nearly all the subsequent elongation occurring in the neck. A few metals and some polymers have a uniaxial behavior in which the nominal stress first peaks but then reaches a minimum and with further straining increases to levels well above the initial peak. Such a uniaxial curve is depicted in Fig. 1(a) where the nominal stress n (load/original area) is shown as a function of the stretch λ (current length/original length). A neck initiates in these materials in much the same way as in typical metal specimens. However, the upturn in the uniaxial nominal stress–strain curve leads to a termination of the localization and forces the neck to spread along the entire length of the specimen as depicted in Fig. 2. An overall load-elongation curve for such a specimen as obtained directly from a test machine record is also sketched in Fig. 2.

Once the neck has started to spread, steady-state propagation conditions are soon approached in which the transition front moves at constant velocity into the unnecked material, assuming a steady overall elongation velocity is imposed. In the steady-state regime the pulling load is constant. Detailed experimental observations of neck initiation and propagation are reported in the recent paper by G'SELL, ALY-HELAL and

JONAS (1982). The phenomenon of neck propagation in polymers is often termed "cold drawing" (WARD, 1971) and is employed as a standard process to harden fibers.

Although neck propagation has been observed for many years, the fundamental mechanical aspects of the problem have not been extensively explored. Thermodynamical features of the problem have been studied by a number of authors including MARSHALL and THOMPSON (1954) and BARENBLATT (1974). While thermal considerations are highly important, the essence of neck propagation lies in its mechanical aspects, and this paper will focus on the mechanics of steady-state neck propagation under conditions in which thermal effects do not need to be explicitly considered. Specifically, it will be assumed that either the propagation is sufficiently rapid such that adiabatic deformation prevails or the propagation is sufficiently slow such that the deformation can be considered to be isothermal.

We begin in the next section by writing down jump, or discontinuity, conditions relating states ahead and behind the neck transition for steady-state propagation. Jump conditions for conservation of mass, momentum and energy are only sufficient to determine the states ahead and behind the transition front when the material is a nonlinear elastic solid. For this reason it is useful to introduce the notion of a fictitious nonlinearly elastic solid with a stress–strain curve such as that in Fig. 1. Results for the nonlinearly elastic solid, which are simply obtainable, will be contrasted with those for an inelastic solid, more typical of polymers or certain metals, whose stress–strain behavior under multiaxial stress histories such as that experienced by a particle passing through the neck transition is inherently path-dependent. For an inelastic solid the jump conditions are not sufficient to determine the deformation states ahead and behind the propagating transition front. To obtain these states a full analysis must be performed, including determination of the shape of the neck transition and the multiaxial deformation history of material elements as they are engulfed by the front. The difference between the elastic and inelastic neck propagation problems is analogous to the difference between shock wave propagation in a gas and that in a solid. The states ahead and behind the shock front can be obtained directly in terms of the jump conditions for a gas characterized by a state function. For shock propagation in an elastic–plastic solid the jump conditions are insufficient to determine the states ahead and behind the shock without knowledge of the constitutive behavior characterizing the multiaxial deformation history of material particles passing through the shock.

The steady-state problem is formulated and solved approximately for propagation of an axisymmetric neck down a circular cylindrical bar. Several material models are considered each of which has uniaxial behavior of the type depicted in Fig. 1. The inelastic material will be represented by J_2 flow theory, both rate-independent and rate-dependent versions. While not necessarily an accurate model of a polymer, the flow theory is sometimes used to represent the multiaxial stress–strain behavior of polymers for lack of anything better. For present purposes it will serve as a prototype material with inelastic features not unlike those expected of a polymer under the multiaxial deformation histories experienced in necking. A similar analysis will also be performed for a nonlinearly elastic solid described by J_2 deformation theory. Since the states ahead and behind the transition can be obtained directly from the jump conditions for this elastic material, this case provides some check on the accuracy of our

approximate three-dimensional analysis. It will also be seen that the predictions for the nonlinearly elastic solid provide a rough approximation for neck propagation along the rate-independent inelastic solid with the same uniaxial stress–strain curve.

2. Steady-state Neck Propagation in an Incompressible Elastic Bar

The bar is assumed to be infinite in extent, to have uniform properties, and to have a uniform cross-section of area A_0 in the undeformed state. The uniaxial stress–strain behavior is of the form graphed in Fig. 1. As already discussed, Fig. 1(a) displays the nominal (engineering) stress, n, as a function of stretch, λ. Figure 1(b) shows the dependence of true stress, σ, on logarithmic strain, $\varepsilon = \ln \lambda$, and this relation is assumed to be monotonically increasing, since we want to exclude any purely material instabilities.

As discussed in the Introduction, the neck is assumed to be propagating under either an adiabatic or an isothermal condition, and the uniaxial behavior in Fig. 1 should be associated with whichever of these conditions is in effect. The full multiaxial stress–strain relation of the elastic solid will not be needed in this section, although it will be assumed that the material possesses a strain energy density function W appropriate to either the adiabatic or isothermal condition.

The results take the simplest form if the material is taken to be incompressible, which will be done. In uniaxial tension, the strain energy density of the material is related to the uniaxial data by

$$W = \int_0^{\lambda} n \, d\lambda = \int_0^{\varepsilon} \sigma \, d\varepsilon. \tag{2.1}$$

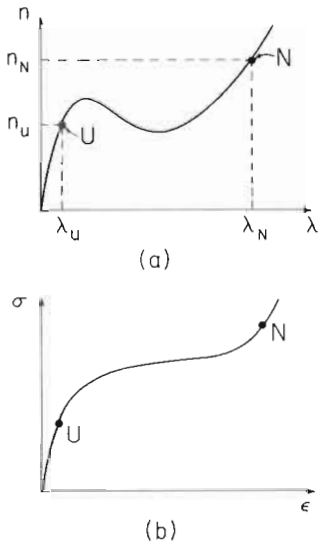

Fig. 1. Uniaxial stress-strain curves. (a) Nominal stress, n, vs. stretch λ. (b) True stress, σ, vs. logarithmic strain, ε.

As depicted in Fig. 2, a neck is assumed to have formed at some point along the bar and then to have spread a distance sufficient to ensure that the transition front joining the necked and unnecked regions is advancing under steady-state conditions. In the idealized steady-state problem shown in Fig. 2 the profile of the bar as well as the stress and strain fields do not change when viewed by an observer travelling at the same velocity as the transition front. The material far ahead of the front is taken to be at rest while the necked section far behind the transition is pulled at velocity v. The transition front moves with velocity c towards the unnecked region.

Far ahead of the transition in the unnecked region the material is in a state of uniaxial tension and we denote the nominal stress and stretch in this state by (n_U, λ_U). Far behind the transition the necked material is also assumed to be in a state of uniaxial tension given by (n_N, λ_N). The state of stress in the transition region is, of course, not uniaxial. However, we do assume that the material behavior is such that no non-smooth behavior occurs in the transition, such as loss of ellipticity. The strain energy density difference between states U and N for a particle passing through the transition is therefore the same as if it experienced a purely uniaxial history between these states since a strain density W is assumed to exist. That is,

$$W_N - W_U = \int_{\lambda_U}^{\lambda_N} n \, d\lambda, \tag{2.2}$$

which is just the area under the uniaxial nominal stress–strain curve between λ_U and λ_N.

Continuity, together with incompressibility, implies

$$c = v\left(\frac{\lambda_N}{\lambda_U} - 1\right)^{-1}. \tag{2.3}$$

If A_U and A_N denote the cross-sectional areas of the bar far ahead and behind the transition, then

$$\lambda_U A_U = \lambda_N A_N = A_0 \tag{2.4}$$

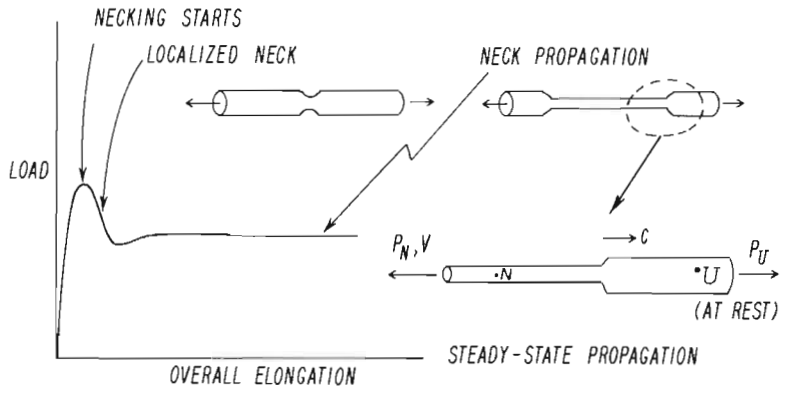

FIG. 2. Overall load-elongation behavior in a tensile test when neck propagation occurs. Conventions for steady-state propagation.

and

$$n_U = P_U/A_0 \quad \text{and} \quad n_N = P_N/A_0 \tag{2.5}$$

where P_U and P_N denote the loads carried at the respective cross-sections.

The rate of change of the momentum of the entire bar in the axial direction is $-cA_U\rho v$ where ρ is the mass density of the bar. Thus, overall momentum balance requires $P_N - P_U = cA_U\rho v$. By using (2.3) to eliminate c and by making use of (2.4) and (2.5), one can write the equation for conservation of momentum as

$$(n_N - n_U)(\lambda_N - \lambda_U) = \rho v^2. \tag{2.6}$$

In a unit of time the pulling load does work $P_N v$, while the transition front has translated forward a distance c. To evaluate the change in kinetic energy and strain energy in the bar during this unit of time, one need only note that to an observer moving with the front the bar appears unchanged. In effect, a segment of volume cA_U from far ahead of the transition has been "transferred" far behind the transition. The increase in kinetic energy is $cA_U\frac{1}{2}\rho v^2$ while the increase in strain energy is $cA_U(W_N - W_U)$. The steady-state energy balance is therefore

$$P_N v = cA_U(W_N - W_U) + \tfrac{1}{2}cA_U\rho v^2. \tag{2.7}$$

Dividing (2.7) by A_0 and using (2.3) through (2.5), one can write the energy balance as

$$n_N(\lambda_N - \lambda_U) = (W_N - W_U) + \tfrac{1}{2}\rho v^2. \tag{2.8}$$

The strain energy density difference in this equation must be interpreted as being associated with either an adiabatic or an isothermal condition, whichever of these limiting conditions is assumed to prevail.

Suppose the pull velocity v is specified. Then equations (2.6) and (2.8), together with the uniaxial strain energy density $W(\lambda)$ in (2.1), fully determine the states (n_U, λ_U) and (n_N, λ_N) ahead and behind the transition, assuming a steady-state solution exists. Furthermore, the velocity of neck propagation c is obtained from (2.3) when λ_N and λ_U have been determined. A graphical solution representing these states is revealing, and for this purpose we use (2.6) to eliminate ρv^2 from (2.8) with the result

$$\tfrac{1}{2}(n_N + n_U)(\lambda_N - \lambda_U) = W_N - W_U. \tag{2.9}$$

Under *quasi-static propagation conditions* when the term ρv^2 can be ignored, (2.6) implies that $n_N = n_U$ or, equivalently, that $P_N = P_U$. With $n_N = n_U \equiv n^*$, (2.9) becomes

$$n^*(\lambda_N - \lambda_U) = W_N - W_U. \tag{2.10}$$

The graphical solution to (2.10) is shown in Fig. 3. By (2.2), $W_N - W_U$ is the area under the curve of n vs. λ between λ_U and λ_N, while $n^*(\lambda_N - \lambda_U)$ is the area of the rectangle superimposed on the figure. The equality of these two areas required by (2.10) is equivalent to the requirement that the areas of the two lobes designated by $\mathscr{R}_1$ and $\mathscr{R}_2$ be equal. In the literature of phase transitions, the horizontal line at n^* connecting the states U and N is called the Maxwell line. The possible relevance of the Maxwell line construction to neck propagation in materials such as polymers was apparently noted by Thompson and Tuckett in the late 1950's or early 1960's (cf. discussion of the paper by BARENBLATT (1974)), but we have been unable to locate this reference.

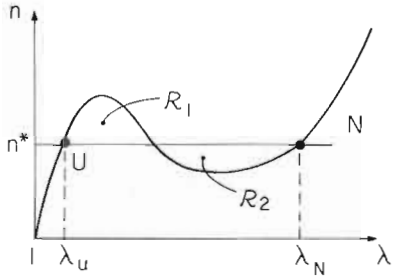

FIG. 3. Maxwell line construction for quasi-static, steady-state neck propagation in an elastic solid.

The quasi-static, steady-state propagation load, $P^* = n^* A_0$, is lower than the peak load, $P_{max} = n_{max} A_0$, that an initially uniform bar can support. This means that the load needed to initiate a neck in a bar is larger than the load needed to propagate the neck quasi-statically once it has started to spread, as has been depicted in Fig. 2.

When ρv^2 is not negligible, (2.6) and (2.9) must be solved simultaneously subject to (2.2). It is straightforward to find the lowest order effect of ρv^2 on the solution by perturbing about the quasi-static solution. An asterisk is used to denote quantities associated with the quasi-static solution from the Maxwell line construction. To lowest order in ρv^2, one finds

$$\begin{aligned} n_N &= n^* + (\lambda_N^* - \lambda_U^*)^{-1} \tfrac{1}{2}\rho v^2 + \cdots \\ n_U &= n^* - (\lambda_N^* - \lambda_U^*)^{-1} \tfrac{1}{2}\rho v^2 + \cdots \\ \lambda_N &= \lambda_N^* + [S_N^*(\lambda_N^* - \lambda_U^*)^{-1}] \tfrac{1}{2}\rho v^2 + \cdots \\ \lambda_U &= \lambda_U^* - [S_U^*(\lambda_N^* - \lambda_U^*)^{-1}] \tfrac{1}{2}\rho v^2 + \cdots \end{aligned} \tag{2.11}$$

where $S \equiv dn/d\lambda$. The pull load, $P_N = n_N A_0$, increases above the quasi-static propagation load as the pull velocity v increases, while the load carried by cross-sections ahead of the transition, $P_U = n_U A_0$, drops. The stretch difference across the transition, $\lambda_N - \lambda_U$, increases with increasing v.

A graphical construction of the solution to (2.6) and (2.9) is also possible when ρv^2 is not negligible, although it is not as pleasingly simple as the Maxwell line construction. Refer to Fig. 4(a), and suppose again that the pull velocity v is prescribed. Equation (2.9) requires that the areas $\mathscr{R}_1$ and $\mathscr{R}_2$ must be equal. In addition, (2.6) requires that U and N must be adjusted such that the area of the rectangle ANBU equals ρv^2.

Some nominal stress–stretch curves result in a maximum pull velocity and load beyond which steady-state propagation ceases to exist, assuming that the bar cannot support compressive loads ahead of the transition. The maximum pull velocity and pull load are associated with the construction shown in Fig. 4(b) where $\lambda_U \to 1$ and λ_N is determined from the condition $\mathscr{R}_1 = \mathscr{R}_2$. Equations (2.6) and (2.9) then reduce to

$$n_N(\lambda_N - 1) = \rho v^2 \quad \text{and} \quad \tfrac{1}{2} n_N(\lambda_N - 1) = W_N \tag{2.12}$$

so that the maximum pull velocity is given by

$$v = \sqrt{(2W_N/\rho)} = \sqrt{[n_N(\lambda_N - 1)/\rho]}. \tag{2.13}$$

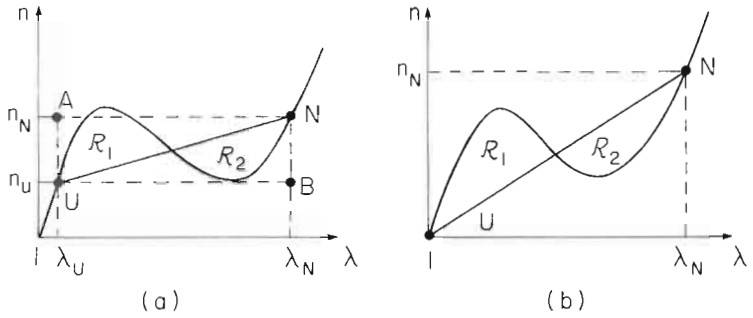

FIG. 4. Graphical construction for dynamic steady-state neck propagation in an elastic solid: (a) general case, (b) corresponding to maximum propagation speed with $n_U = 0$.

In a later section, a numerical example will illustrate the occurrence of a maximum pull velocity in a nonlinearly elastic bar.

3. Three-Dimensional Analysis of Steady-state Neck Propagation

In the previous section it was possible to determine the states on either side of the transition, independently of the details of the behavior in the transition, because the strain energy difference $W_N - W_U$ could be determined in terms of the uniaxial states U and N. This is not the case for an inelastic solid. Because the stress–strain behavior of an inelastic solid is inherently path-dependent, substantial deviations of the stressing history from uniaxial states in the transition region render invalid the calculation of $W_N - W_U$ from uniaxial data alone. For an inelastic solid it is essential to analyze the full three-dimensional problem to obtain the states on either side of the transition.

The equations of conservation of mass (2.3), momentum (2.6) and energy (2.8) derived in the previous section continue to hold for steady-state propagation along an incompressible inelastic bar. Now, however, n_N must be interpreted as the nominal stress averaged across the cross-section (i.e., P_N/A_0), while $W_N - W_U$ is the stress–work experienced by a cross-sectional slice of unit volume as it passes through the transition. We will make use of these jump conditions later.

The three-dimensional analysis of steady-state neck propagation is carried out for an infinitely long round bar made of an incompressible material with a uniaxial true stress–true strain ($\sigma - \varepsilon$) and nominal stress–stretch (n, λ) curve similar to those depicted in Fig. 1. The multiaxial constitutive relations will be detailed in the next section.

A cylindrical polar coordinate system (r, θ, z) is used as a reference. Without loss of generality we take this system to be situated in the transition front and to be translating with it along the bar axis at a constant velocity c (Fig. 5). Because of axisymmetry the particle velocities become

$$\mathbf{v} = v_r \mathbf{e}_r + v_z \mathbf{e}_z, \tag{3.1}$$

where $\mathbf{e}_r$, $\mathbf{e}_z$ are unit base vectors in the r and z directions, respectively, and the components v_r, v_z are functions of r and z only. The boundary conditions on these

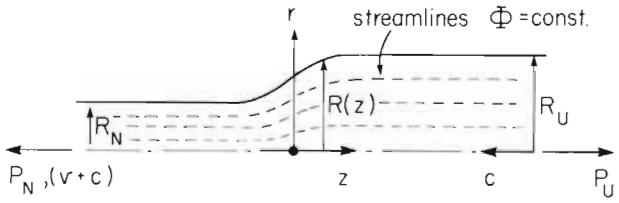

FIG. 5. Conventions for analysis of axisymmetric steady-state neck propagation.

components are the same as those considered in the previous section except that they are expressed in the coordinate system translating with the front, namely

$$\begin{aligned} v_r &= 0, \quad v_z = -c \qquad \text{as } z \to +\infty, \\ v_r &= 0, \quad v_z = -(v+c) \quad \text{as } z \to -\infty. \end{aligned} \tag{3.2}$$

The profile of the bar during neck propagation is such that the cross-sections become uniform far away from the transition front with a radius $R(z) = R_U$ as $z \to +\infty$ and $R = R_N$ as $z \to -\infty$ and the slopes $R'(z)$ approaching zero as $z \to \pm\infty$. Since $\lambda_N/\lambda_U = (R_U/R_N)^2$ the continuity relation (2.3) becomes

$$v = c\left[\left(\frac{R_U}{R_N}\right)^2 - 1\right]. \tag{3.3}$$

The Eulerian strain-rate components associated with the axisymmetric velocity field (3.1) are as follows

$$\begin{aligned} &\dot{\varepsilon}_{rr} = v_{r,r}, \quad \dot{\varepsilon}_{\theta\theta} = \frac{v_r}{r}, \quad \dot{\varepsilon}_{zz} = v_{z,z}, \\ &\dot{\varepsilon}_{rz} = \frac{1}{2}(v_{r,z} + v_{z,r}), \quad \dot{\varepsilon}_{r\theta} = \dot{\varepsilon}_{z\theta} = 0, \end{aligned} \tag{3.4}$$

where a comma denotes partial differentiation. Incompressibility requires that $\dot{\varepsilon}_{rr} + \dot{\varepsilon}_{\theta\theta} + \dot{\varepsilon}_{zz} = 0$. This constraint can be satisfied by introducing a stream function $\Phi(r, z)$ such that

$$v_r = \frac{1}{r}\Phi_{,z}, \quad v_z = -\frac{1}{r}\Phi_{,r}. \tag{3.5}$$

Curves $\Phi = \text{const.}$ identify the streamlines of the flow. The strain-rate components (3.4) are then given by

$$\begin{aligned} \dot{\varepsilon}_{rr} &= -\frac{1}{r^2}\Phi_{,z} + \frac{1}{r}\Phi_{,rz}, \\ \dot{\varepsilon}_{\theta\theta} &= \frac{1}{r^2}\Phi_{,z}, \quad \dot{\varepsilon}_{zz} = -\frac{1}{r}\Phi_{,rz}, \\ \dot{\varepsilon}_{rz} &= \frac{1}{2r}\left[\Phi_{,zz} - \Phi_{,rr} + \frac{1}{r}\Phi_{,r}\right]. \end{aligned} \tag{3.6}$$

variational principle (3.7). We have $\bar{R} = \bar{R}(\bar{R}_N, c_i)$ $i = 1, \ldots, k$ so that

$$\begin{aligned}
\delta\bar{R} &= \sum_{i=0}^{k} \frac{\partial \bar{R}}{\partial c_i}\delta c_i \equiv \sum_{i=0}^{k} \bar{R}_i \delta c_i, \\
\delta\bar{R}' &= \sum_{i=0}^{k} \frac{\partial \bar{R}'}{\partial c_i}\delta c_i \equiv \sum_{i=0}^{k} \bar{R}_i' \delta c_i, \\
\delta\bar{R}'' &= \sum_{i=0}^{k} \frac{\partial \bar{R}''}{\partial c_i}\delta c_i \equiv \sum_{i=0}^{k} \bar{R}_i'' \delta c_i.
\end{aligned} \tag{3.13}$$

(Note that $\bar{R}_i' \equiv \partial\bar{R}'/\partial c_i$ is not equal to $(\bar{R}_i)'$ in general, and similarly that $\bar{R}_i'' \equiv \partial\bar{R}''/\partial c_i \neq (\bar{R}_i)''$. Above and in the following, $c_0 \equiv \bar{R}_N$.)

From (3.11) to (3.13) and the relation $s_{kk} = 0$ we obtain the following for the integrand in (3.7).

$$s_{ij}\delta\dot{\varepsilon}_{ij} + \rho a_i \delta v_i = \frac{c}{R_U}\sum_{i=0}^{k}[f_0\bar{R}_i + f_1\bar{R}_i' + f_2\bar{R}_i'']\delta c_i + \frac{f_3}{R_U}\delta c, \tag{3.14}$$

with

$$\begin{aligned}
f_0 &= -\frac{1}{\bar{R}^4}\left[9s_{zz}\bar{R}' + s_{rz}\bar{r}\left(\frac{4\psi}{\bar{R}} + \bar{R}''\right)\right] + \frac{\rho c^2}{\bar{R}^8}\left[\frac{3\bar{r}^2\omega}{\bar{R}^2} - 4\right]\bar{R}', \\
f_1 &= \frac{3}{\bar{R}^3}\left[s_{zz} + 2s_{rz}\bar{R}'\frac{\bar{r}}{R}\right] - \frac{\rho c^2}{\bar{R}^9}\bar{r}^2\omega, \\
f_2 &= -\frac{1}{\bar{R}^3}s_{rz}\bar{r}, \\
f_3 &= \frac{1}{\bar{R}^3}\left[3s_{zz}\bar{R}' + s_{rz}\psi\frac{\bar{r}}{\bar{R}}\right] + \frac{\rho c^2}{\bar{R}^7}\left[2 - \frac{\bar{r}^2\omega}{\bar{R}^2}\right]\bar{R}'
\end{aligned} \tag{3.15}$$

and

$$\psi = 3(\bar{R}')^2 - \bar{R}\bar{R}'', \quad \omega = \bar{R}\bar{R}'' - 2(\bar{R}')^2. \tag{3.16}$$

The continuity relation (3.3) gives the connection

$$\delta v = -\frac{2c}{\bar{R}_N^3}\delta\bar{R}_N + \left(\frac{1}{\bar{R}_N^2} - 1\right)\delta c. \tag{3.17}$$

By setting the coefficients of $\delta\bar{R}_N$, δa_i and δc equal to zero in (3.7) we obtain the following set of equations

$$\begin{aligned}
h_0 &= \frac{P_N}{A_U} + \int_{-\infty}^{\infty}[g_0\bar{R}_0 + g_1\bar{R}_0' + g_2\bar{R}_0'']\,\mathrm{d}\bar{z} = 0, \\
h_i &= \int_{-\infty}^{\infty}[g_0\bar{R}_i + g_1\bar{R}_i' + g_2\bar{R}_i'']\,\mathrm{d}\bar{z} = 0, \quad i = 1, \ldots, k, \\
h_{(k+1)} &= \frac{\bar{R}_N}{2A_U}(P_N - P_U\bar{R}_N^2) - \int_{-\infty}^{\infty} g_3\,\mathrm{d}\bar{z} = 0,
\end{aligned} \tag{3.18}$$

where

$$g_i = \bar{R}_N^3 \int_0^{\bar{R}(z)} f_i \bar{r}\, d\bar{r}, \quad i = 0, \ldots, 3. \tag{3.19}$$

The last equation of the set (3.18) can be written as

$$P_N v = \int_V s_{ij}\dot{\varepsilon}_{ij}\, dV + \tfrac{1}{2} c A_U \rho v^2, \tag{3.20}$$

where V is the volume. This is simply the work balance which is equivalent to the relation (2.7).

Consider the pull velocity v as the prescribed quantity. Equations (3.18) together with the continuity relation (3.3) and the momentum balance relation (3.9) then provides a set of $(k+4)$ equations for the $(k+4)$ parameters P_N, P_U, $c, \bar{R}_N$ and c_i $(i = 1, \ldots, k)$.

Numerical results will later be given for the following two-parameter description of the bar profile

$$\bar{R}(\bar{z}) = \tfrac{1}{2}[(1+\bar{R}_N)+(1-\bar{R}_N)\tanh(\beta\bar{z})], \tag{3.21}$$

where $c_1 \equiv \beta$ is a measure of the sharpness of the transition front. The profile (3.21) satisfies the boundary conditions at $z = \pm\infty$. Substituting (3.21) into (3.18) and substituting for P_N and c using (3.9) and (3.3) gives three equations of the form (3.18) to determine P_U, $\bar{R}_N = R_N/R_U$ and β for a prescribed pull velocity v. Once the values of P_U, R_N and β have been computed, we go back to (3.9) and (3.3) to determine P_N and the neck speed c.

4. Constitutive Laws

The constitutive laws employed in the three-dimensional analysis are finite strain versions of the classical J_2 flow and J_2 deformation theories of plasticity. As mentioned previously, the flow theory solid will serve as a prototype material to characterize the inelastic features of neck propagation even though it is perhaps not entirely adequate for describing the real multiaxial behavior of polymers at large strains. Since deformation theory describes a true nonlinear elastic solid, it will serve to verify the accuracy of our three-dimensional numerical solutions as the exact solutions for the loads P_N, P_U and radius reduction R_N/R_U in this case are given by the analysis of Section 2.

J_2 Flow theory

We assume the material to be rigid–plastic and first consider time-independent material behavior. For continuing yielding the J_2 flow theory constitutive law is

$$s_{ij} = \frac{2}{3}\frac{\sigma_e}{\dot{\bar{\varepsilon}}}\dot{\varepsilon}_{ij}, \tag{4.1}$$

where

$$\sigma_e = (\tfrac{3}{2}s_{ij}s_{ij})^{1/2}, \quad \dot{\bar{\varepsilon}} = (\tfrac{2}{3}\dot{\varepsilon}_{ij}\dot{\varepsilon}_{ij})^{1/2} \tag{4.2}$$

are the effective stress and effective strain-rate, respectively. The effective strain $\bar{\varepsilon}$ is defined as $\int \mathrm{d}\bar{\varepsilon}$. In simple tension the effective stress and effective strain are equal to the true stress σ and logarithmic strain ε, respectively. The σ_e–$\bar{\varepsilon}$ curve for uniaxial tension is assumed to hold for multiaxial stress histories. A true stress–natural strain curve with the features illustrated in Fig. 1(b) will be employed in this analysis. This rate-independent curve is written as

$$\sigma_e = \bar{\sigma}_s(\bar{\varepsilon}) \tag{4.3}$$

with no dependence on effective strain-rate $\dot{\bar{\varepsilon}}$.

To describe rate-dependent material response, we replace (4.3) in the flow theory equations (4.1) by the following relation

$$\sigma_e = \sigma_s(\bar{\varepsilon})\left[1 + m \ln\left(1 + \frac{\dot{\bar{\varepsilon}}}{\dot{\varepsilon}_R}\right)\right], \tag{4.4}$$

where m is a strain-rate hardening index and $\dot{\varepsilon}_R$ is a reference strain-rate. The above curve (4.4) reduces to the time-independent relation (4.3) when $m = 0$ and in the quasi-static limit ($\dot{\bar{\varepsilon}} \to 0$). A relation of the form (4.4) brings in the effect of material strain-rate dependence in the simplest possible way, and it cannot be expected to accurately represent material behavior for arbitrary histories of stress, strain and strain-rate. This model should be sufficient, however, for giving a qualitative indication of the effects of material rate-sensitivity on neck propagation.

For the steady-flow problem formulated in the previous section, the fields $\dot{\varepsilon}_{ij}$, $\dot{\bar{\varepsilon}}$ are specified by the wave speed c and profile of the bar $R(z)$. To determine the spatial distribution of effective strain $\bar{\varepsilon}$ we note first that $\bar{\varepsilon} = \varepsilon_U = \ln \lambda_U$ at $z = \infty$ and then integrate along the streamlines $\Phi = \text{const.}$ as follows:

$$\bar{\varepsilon} = \varepsilon_U + \int_\infty^{(r,z)} \frac{\dot{\bar{\varepsilon}}}{|\mathbf{v}|}\,\mathrm{d}l, \tag{4.5}$$

where $\mathrm{d}l = |\mathbf{v}|\ \mathrm{d}z/v_z = |\mathbf{v}|\ \mathrm{d}r/v_r$ represents an element of arc length along the streamline. For the fields corresponding to (3.10) we have

$$\bar{\varepsilon} = \varepsilon_U - \int_\infty^{\bar{z}} \frac{1}{\bar{R}}\left\{4(\bar{R}')^2 + \frac{1}{3}\left(\frac{\bar{r}}{\bar{R}}\right)^2 [3(\bar{R}')^2 - \bar{R}\bar{R}'']^2\right\}^{1/2} \mathrm{d}\bar{z}, \tag{4.6}$$

where here $\bar{r} \equiv \bar{r}(z)$ is the radial coordinate along the particular streamline considered. Having computed the $\bar{\varepsilon}$ distribution, we can calculate the value of the effective stress σ_e at each point using (4.3) or (4.4) and then substitute in (4.1) to compute stress deviator components s_{ij}.

J_2 Deformation theory

The finite strain J_2 deformation theory constitutive law considered is a nonlinear elastic law for isotropic, incompressible solids. Aspects of this law were discussed in

previous papers (HUTCHINSON and NEALE, 1978, 1981). In applying it here we make use of Hill's theory and "principal-axes techniques" (HILL, 1970) for finitely deformed isotropic elastic solids.

Let s_i and $\varepsilon_i = \ln \lambda_i$ denote the principal components of Cauchy stress deviator and principal logarithmic strains, respectively (λ_i are the principal stretches). The logarithmic strain tensor $\boldsymbol{\varepsilon}$ is, by definition, coaxial with the Lagrangian strain ellipsoid. Furthermore, the strain-rates $\dot{\varepsilon}_1$, etc. are identically equal to the Eulerian strain-rate components $\dot{\varepsilon}'_{11}$, etc. referred to the current axes (x'_1, x'_2) of the Eulerian strain ellipsoid. Transforming the strain-rate components from the (z, r) reference system to the principal Eulerian axes (x'_1, x'_2) one finds

$$\begin{aligned}
\dot{\varepsilon}_1 &= \dot{\varepsilon}'_{11} = \tfrac{1}{2}[(\dot{\varepsilon}_{zz}+\dot{\varepsilon}_{rr})+(\dot{\varepsilon}_{zz}-\dot{\varepsilon}_{rr})\cos 2\phi]+\dot{\varepsilon}_{rz}\sin 2\phi,\\
\dot{\varepsilon}_2 &= \dot{\varepsilon}'_{22} = \tfrac{1}{2}[(\dot{\varepsilon}_{zz}+\dot{\varepsilon}_{rr})-(\dot{\varepsilon}_{zz}-\dot{\varepsilon}_{rr})\cos 2\phi]-\dot{\varepsilon}_{rz}\sin 2\phi,\\
\dot{\varepsilon}'_{12} &= -\tfrac{1}{2}(\dot{\varepsilon}_{zz}-\dot{\varepsilon}_{rr})\sin 2\phi+\dot{\varepsilon}_{rz}\cos 2\phi,
\end{aligned} \tag{4.7}$$

where ϕ represents the orientation of the x'_1-axis with respect to z-axis. HILL (1970) gives the following for the rate of rotation of the principal Eulerian axes:

$$\dot{\phi} = \frac{\lambda_1^2+\lambda_2^2}{\lambda_1^2-\lambda_2^2}\dot{\varepsilon}'_{12}+\dot{\Omega}, \tag{4.8}$$

where $\dot{\Omega} = (v_{r,z}-v_{z,r})/2$ represents the rigid-body spin of a material element in the z–r plane. By integrating along streamlines as described earlier, we get

$$\begin{aligned}
\phi &= \phi^{\mathrm{U}} - \int_{\infty}^{z}\left[\frac{R(z)}{R_{\mathrm{U}}}\right]^2\frac{\dot{\phi}}{c}\,\mathrm{d}z,\\
\varepsilon_i &= \varepsilon_i^{\mathrm{U}} - \int_{\infty}^{z}\left[\frac{R(z)}{R_{\mathrm{U}}}\right]^2\frac{\dot{\varepsilon}_i}{c}\,\mathrm{d}z,
\end{aligned} \tag{4.9}$$

where $\phi^{\mathrm{U}} = 0$, $\varepsilon_1^{\mathrm{U}} = \varepsilon_{\mathrm{U}}$, and $\varepsilon_2^{\mathrm{U}} = -\varepsilon_{\mathrm{U}}/2$ designate the values at $z = \infty$.

To determine the current stress deviator components we make use of the fact that, for an isotropic elastic solid, the principal directions of the Cauchy deviatoric stress tensor $\mathbf{s}$ must coincide with the principal Eulerian axes x'_i. The finite strain J_2 deformation theory law is expressed in terms of the principal components of $\mathbf{s}$ and $\boldsymbol{\varepsilon}$ and has the form (HUTCHINSON and NEALE, 1978)

$$s_i = \frac{2}{3}\frac{\sigma_{\mathrm{e}}}{\varepsilon_{\mathrm{e}}}\varepsilon_i, \tag{4.10}$$

where the effective strain ε_{e} is defined as follows

$$\varepsilon_{\mathrm{e}} = \left(\frac{2}{3}\varepsilon_i\varepsilon_i\right)^{1/2}. \tag{4.11}$$

The effective stress and strain are related by the uniaxial relation (4.3), i.e. $\sigma_{\mathrm{e}} = \sigma_{\mathrm{s}}(\varepsilon_{\mathrm{e}})$. Thus for a given flow field (prescribed by the wave speed c and radius profile $R(z)$) we can integrate (4.9) along the streamlines $\Phi = \text{const.}$ to determine the principal axes orientations ϕ and total principal strains ε_i. Equations (4.10), (4.11) together with the uniaxial stress–strain relation (4.3) gives the principal stress deviators s_i. Transforming

back to the (z, r) reference system gives

$$s_{zz} = \tfrac{1}{2}[(s_1+s_2)+(s_1-s_2)\cos 2\phi],$$
$$s_{rr} = \tfrac{1}{2}[(s_1+s_2)-(s_1-s_2)\cos 2\phi], \tag{4.12}$$
$$s_{rz} = \tfrac{1}{2}(s_1-s_2)\sin 2\phi.$$

Other schemes are possible for analyzing the nonlinear elastic solid which would more naturally exploit the path-independence of the material. However, the present scheme was used because it fits in with the numerical approach outlined in the previous section.

5. Results and Discussion

Some characteristic features of neck propagation in elastic and inelastic materials will now be examined. Numerical results have been generated using the analyses of the previous sections. Details of the numerical procedure associated with the three-dimensional analysis are discussed in the Appendix.

The particular form of uniaxial stress–strain curve (4.3) adopted was constructed by modifying the experimental relation suggested by G'Sell and Jonas (1979) as follows:

$$\sigma = \begin{cases} \alpha k \varepsilon^N & \text{for } \varepsilon \leqslant \varepsilon_0, \\ k \exp(M\varepsilon^2) & \varepsilon \geqslant \varepsilon_0. \end{cases} \tag{5.1}$$

We take k, ε_0 and M as the independent material constants and impose continuity of the stress σ and tangent modulus $d\sigma/d\varepsilon$ at $\varepsilon = \varepsilon_0$. This gives $N = 2M(\varepsilon_0)^2$ and $\alpha = \exp(N/2)/\varepsilon_0^N$. The uniaxial nominal stress–stretch curve associated with (5.1) reaches a local maximum when $\varepsilon = N$, a local minimum when $\varepsilon = 1/(2M)$ and thus has the form depicted in Fig. 1(a) if $N < \varepsilon_0 < 1/(2M)$. Numerical results will be given for two cases: (i) $M = 0.50, \varepsilon_0 = 0.50$ and (ii) $M = 0.25, \varepsilon_0 = 1.00$. The uniaxial curves associated with these choices are shown in Fig. 6 where the peaks are $n_{max}/k = P_{max}/(kA_0) = 0.742$ and 0.551, respectively.

Results are first given for dynamic steady-state neck propagation in rate-independent nonlinearly elastic and inelastic materials (Figs 7–10). In Figs 7 and 8 the loads P_N/P_{max} and P_U/P_{max} are plotted against the nondimensional parameter $\zeta = \rho v^2/k$ which is associated with the pull velocity. Solid curves here refer to the inelastic material (J_2 flow theory) while dashed curves refer to the nonlinear elastic solid (J_2 deformation theory). These results emanate from the three-dimensional analysis of Section 3. The dash–dotted curves represent the exact solutions for the same nonlinear elastic material as obtained from the analysis of Section 2. (This curve for P_N in Fig. 7 is indistinguishable from the dashed curve.) The close agreement between the exact results and those obtained numerically for the nonlinear elastic material suggests that the discretization and associated integration formulas of the numerical scheme used in conjunction with the three-dimensional analysis are reasonably accurate.

When the material behavior is elastic the loads P_N and P_U respectively increase and decrease monotonically with increasing pull velocity v (Figs 7 and 8), as suggested by the graphical construction of Fig. 4. A maximum pull velocity corresponding to $P_U = 0$

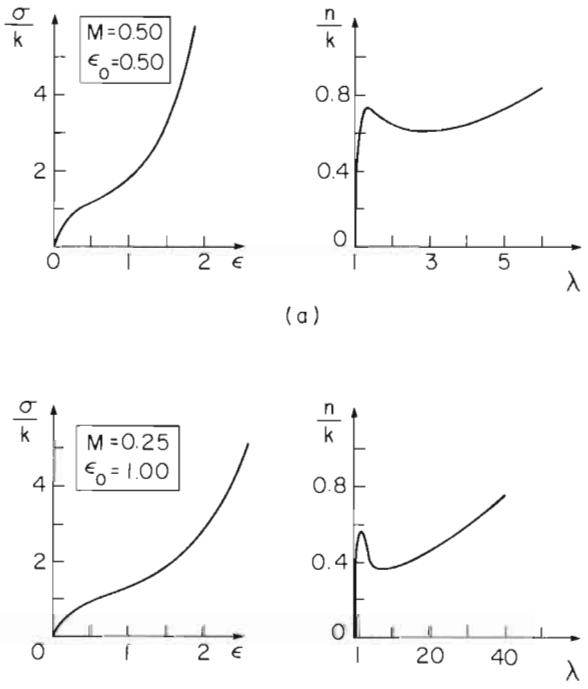

FIG. 6. Uniaxial stress–strain curves used in numerical calculations.

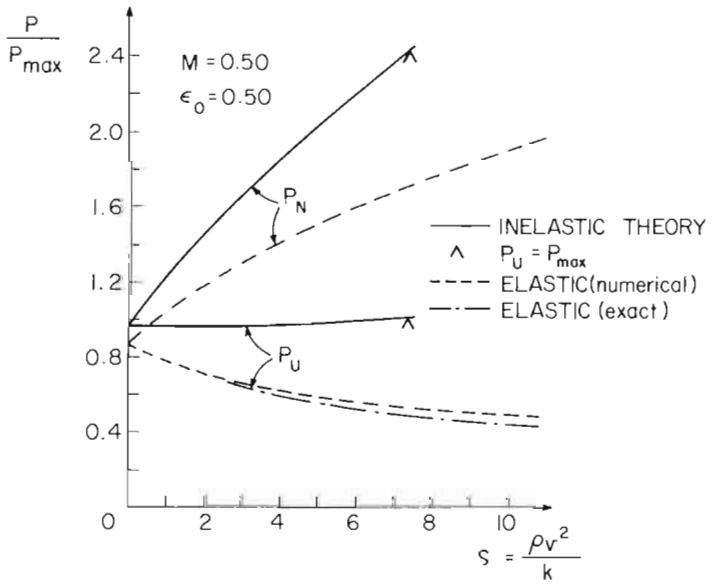

FIG. 7. Normalized loads as a function of pull velocity parameter ζ.

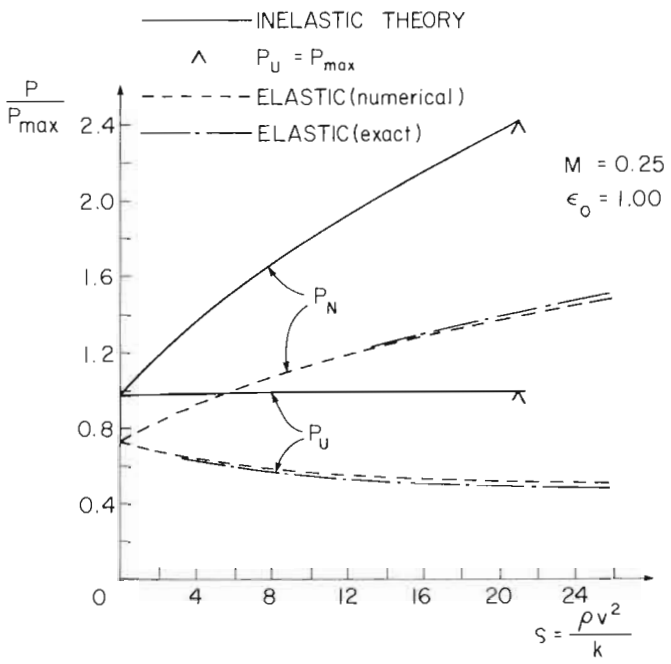

FIG. 8. Normalized loads as a function of pull velocity parameter ζ.

is eventually attained, although only at large ζ. When the material behavior is inelastic, the load carried by cross-sections far behind the transition front P_N also experiences an increase with increasing pull velocity. However, the load in the unnecked region far ahead of the wave front P_U first decreases very slightly with increasing velocity but then begins to increase. A value of velocity is eventually reached where $P_U = P_{max}$, that is, where the nominal uniaxial tensile stress in the unnecked sections is at the maximum point on the n–λ curve of the material. This state, designated by a $\hat{}$, would permit the onset of localized necking in the region ahead of the transition. Our solution cannot encompass such behavior and our curves have been terminated when $P_U = P_{max}$.

The results shown in Figs 7 and 8 indicate that, for a prescribed pull velocity, the inelastic material requires a higher pull load than the elastic material. This is to be expected since the energy which is dissipated in the transition region due to shearing is not recovered in the inelastic solid. In the quasi-static limit $\zeta = 0$, $P_U = P_N$ and the elastic solution is that given by the Maxwell-line construction. The load level for quasi-static propagation in the inelastic material is again higher than that for the elastic material.

As discussed earlier, (2.9) holds for the inelastic solid as well as the elastic solid if $W_N - W_U$ is understood to be the average stress–work absorbed by a cross-sectional slice of unit volume as it passes through the transition. By (2.9) the ratio of the average stress-work experienced by the inelastic material to that of the elastic material is

$$\frac{(W_N - W_U)_{\text{inelastic}}}{(W_N - W_U)_{\text{elastic}}} = \frac{[(n_N + n_U)(\lambda_N - \lambda_U)]_{\text{inelastic}}}{[(n_N + n_U)(\lambda_N - \lambda_U)]_{\text{elastic}}}. \tag{5.2}$$

For the material with $M = 0.5$ and $\varepsilon_0 = 0.5$, this ratio ranges from 1.32 in the quasi-static limit to 1.26 for $\rho v^2/k = 7.4$. For the second material ($M = 0.25$, $\varepsilon_0 = 1.0$), the range is 1.26 for $\rho v^2 = 0$–1.12 for $\rho v^2 = 20.9$. In quasi-static propagation the inelastic material absorbs about 30% more energy than the corresponding fictitious nonlinearly elastic material.

Plots of the radius-reduction ratio R_N/R_U and transition profile parameter β against the pull velocity parameter ζ are shown in Figs 9 and 10. Figure 9 indicates that the ratio R_N/R_U for the elastic material is generally less than that for the inelastic solid, and that this ratio decreases with increasing pull velocity for both materials. Correspondingly, the β-parameter increases with increasing ζ (Fig. 10) with the elastic solid exhibiting an increasingly sharper transition profile (higher β value) than the inelastic solid.

Although the cold drawing of polymers is a high speed process, generally the rate of neck propagation is still not fast enough for inertial effects to be important. On the other hand, polymers have a positive rate-dependence and velocity effects can therefore appear even in quasi-static propagation. The results presented below were determined

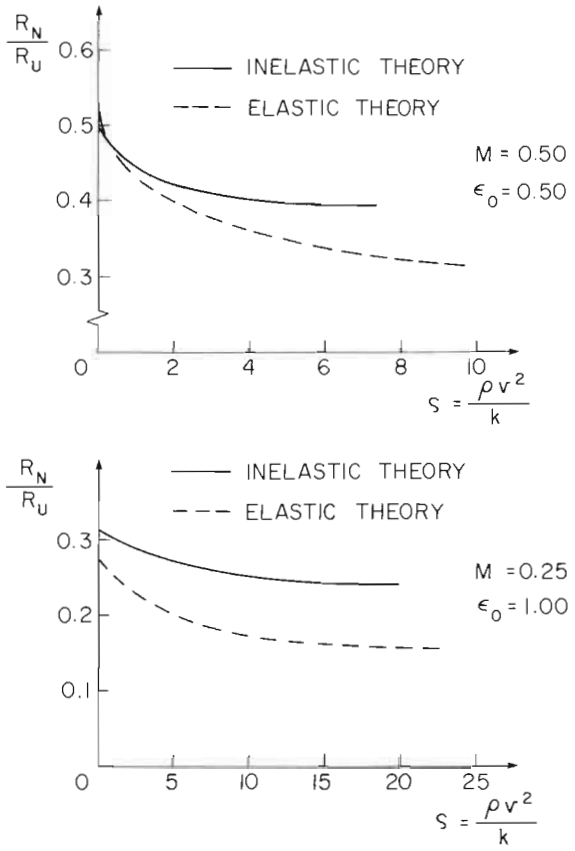

FIG. 9. Ratio of radius behind transition to radius ahead of transition as a function of pull velocity parameter.

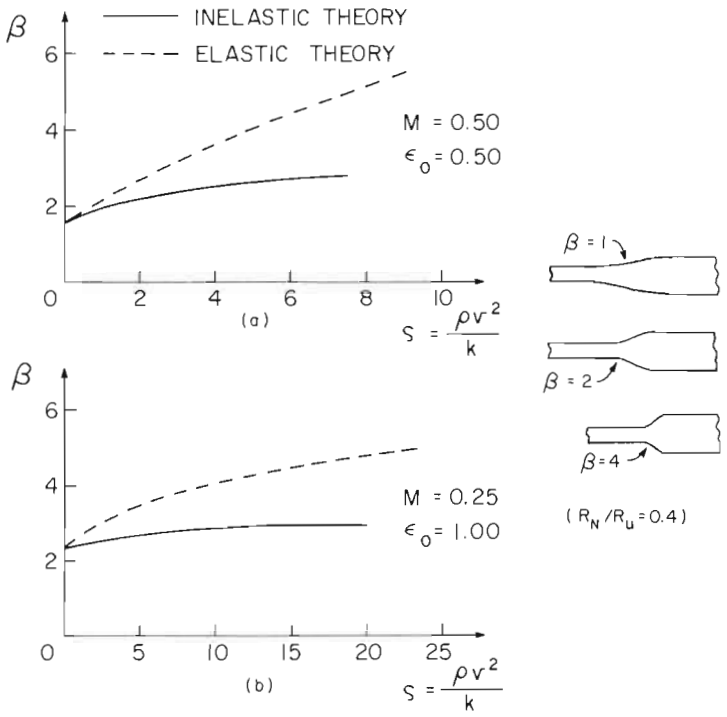

FIG. 10. Variation of the transition width parameter (see equation (3.21)) with pull velocity parameter.

neglecting inertial effects. The rate-dependent relation (4.4) was assumed in conjunction with the flow law (4.1). Two values of the strain-rate sensitivity have been considered: $m = 0.01$ and 0.05. The non-dimensional velocity parameter which arises in this analysis is $\gamma = v/(R_U\dot{\varepsilon}_R)$. Plots of the pull load, the radius-reduction and the transition width parameter β as functions of γ are given in Figs 11–14. In these figures P_{max} is the peak load ($n_{max}A_0$) associated with $m = 0$ or, equivalently, associated with $\dot{\bar{\varepsilon}}/\dot{\varepsilon}_R \to 0$. A higher load level is required to increase the pull velocity, yet the transition profile becomes smoother (β decreases) accompanied by a slightly smaller reduction in radius (R_N/R_U increases).

The mathematical character of the steady-state rate-independent problem is different from the corresponding rate-dependent problem. In the rate-independent problem the quasi-static pull load is independent of the pull velocity. The mathematical problem for P^* is a nonlinear eigenvalue problem. When rate-dependence is present the pull load is a function of the pull velocity v. The rate-dependent results of Figs 11–14 coincide with the quasi-static time-independent results as $v \to 0$ since (4.4) reduces to the time-independent relation as $\dot{\bar{\varepsilon}}/\dot{\varepsilon}_R \to 0$.

A positive strain-rate sensitivity ($m > 0$) has the expected effect of stabilizing neck propagation. For example, once a neck is initiated and starts to spread it will tend to propagate in both directions, as depicted in Fig. 2 and as is usually observed experimentally. Any tendency for either one of the propagating transition fronts to slow down is offset by a drop in flow resistance and *vice versa*.

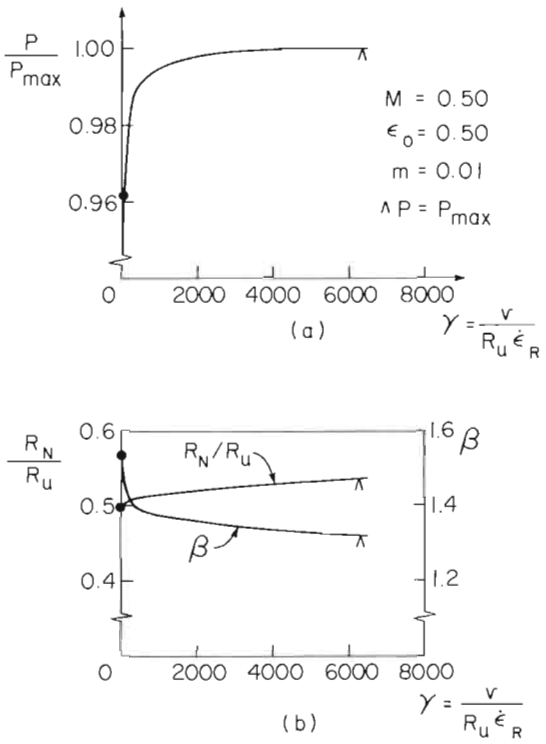

FIG. 11. Results for quasi-static, steady-state neck propagation in rate-dependent inelastic solid.

Another feature which emerges in Figs 11–14 is the increase of the pull load towards P_{max} with increasing pull velocity. When the pull load is very close to P_{max} there will be a tendency for necks to initiate ahead of the travelling front at any section with a slight reduction in cross-sectional area (or material strength) due to an initial nonuniformity in the fiber. The approach of the pull load toward P_{max} with increasing γ is rather

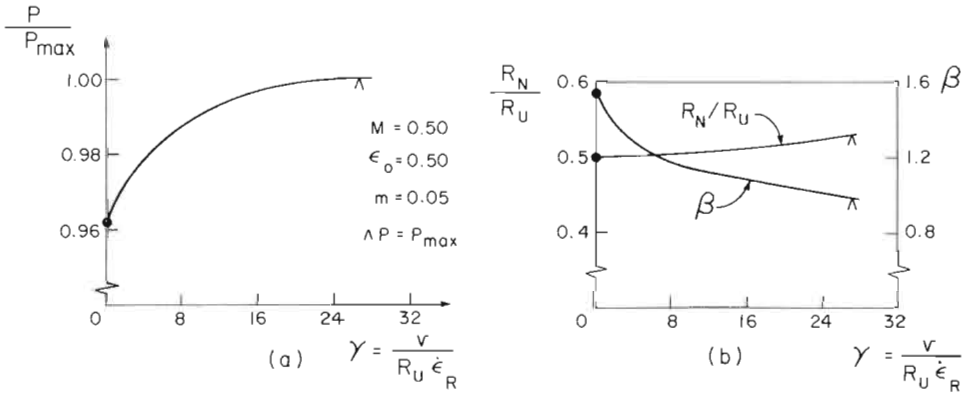

FIG. 12. Results for quasi-static, steady-state neck propagation in rate-dependent inelastic solid.

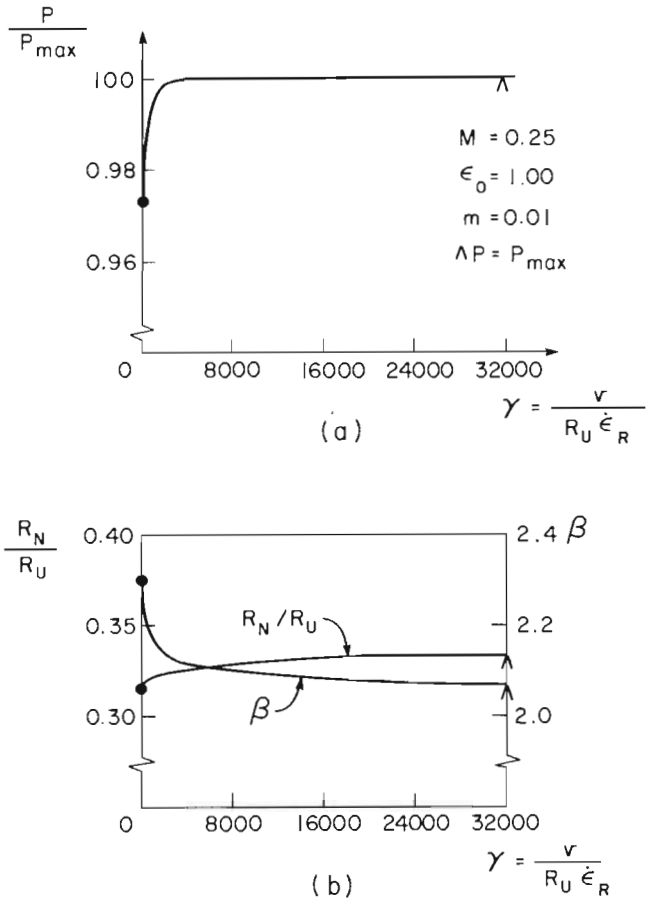

FIG. 13. Results for quasi-static, steady-state neck propagation in rate-dependent inelastic solid.

gradual. Thus, it may be difficult to identify a precise value of γ where multiple necks will start to be observed.

6. CONCLUDING REMARKS

Qualitative insight into neck propagation along polymers is gained from the analysis based on the fictitious nonlinear elastic solid, but quantitative predictions require that inelasticity be taken into account. The present analysis can be improved upon in a number of respects. First, there is no obstacle to incorporating other, more realistic, constitutive descriptions of material behavior. Secondly, the accuracy of the three-dimensional solution can be improved upon if that seems warranted. The improvement which would involve the least alteration to the scheme used here would be the inclusion of more free parameters in the specification of the shape of the neck transition. It is also possible that the approximate form (3.10) of the stream function assumed here is too

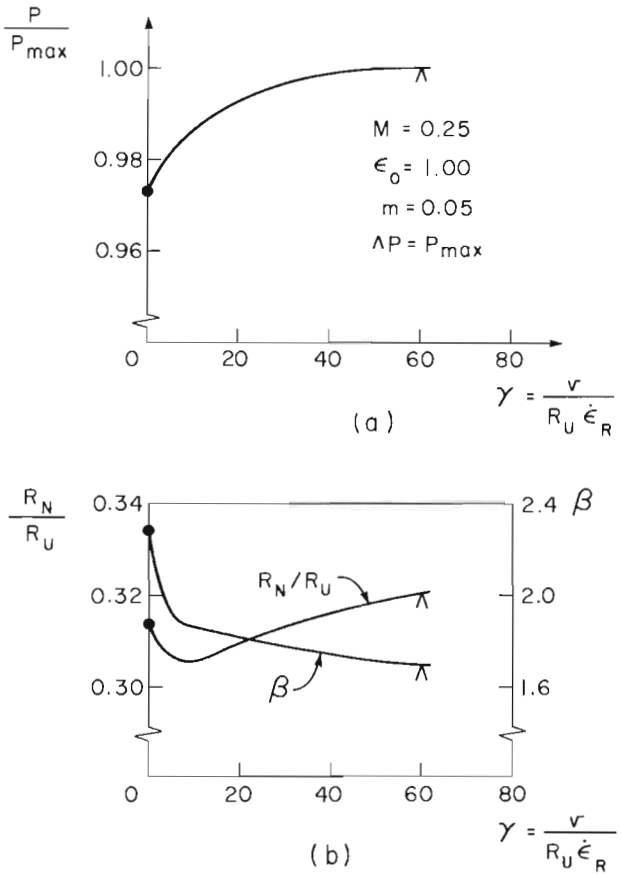

FIG. 14. Results for quasi-static, steady-state neck propagation in rate-dependent inelastic solid.

restrictive. In principle, this choice could be generalized as well, but with a sacrifice of some of the simplicity.

Tensile specimens of some metals propagate necks, or bands, along their length. A well-known example is the propagation of Lüders bands in mild steel. While there are a number of similarities between Lüders band propagation and the neck propagation discussed in this paper, there is an essential difference. Mild steel displays a true material instability at its upper yield point. In uniaxial tension the true stress, as well as the nominal stress, peaks at the upper yield point, and this precipitates the shear band formation characteristic of Lüders bands. In the present paper we have restricted attention to materials which do not undergo material shear instabilities, at least over the range of deformation states considered.

ACKNOWLEDGEMENTS

We are indebted to C. G'Sell who first aroused our interest in neck propagation and to U. F. Kocks for helpful discussion. The work of J.W.H. was supported in part by the National Science

Foundation under Grant MEA-82-13925, and by the Division of Applied Sciences, Harvard University. The work was initiated while K.W.N. was on sabbatical leave at Harvard University, and was supported in part by the Faculty of Applied Sciences at the University of Sherbrooke, and by the Division of Applied Sciences, Harvard University.

REFERENCES

BARENBLATT, G. I.	1974	In *Deformation and Fracture of High Polymers* (edited by H. H. RAUSCH, J. A. HASSELL and R. I. JAFFEE p. 91. Plenum Press, New York.
G'SELL, C. and JONAS, J. J.	1979	*J. Mater. Sci.* **14,** 583.
G'SELL, C., ALY-HELAL, N. A. and JONAS, J. J.	1983	*J. Mater. Sci.*, in press.
HILL, R.	1970	*Proc. R. Soc. A***314,** 457.
HUTCHINSON, J. W. and NEALE, K. W.	1978	In *Mechanics of Sheet Metal Forming*, (edited by D. P. KOISTINEN and N-M. WANG) p. 127. Plenum Press, New York.
	1981	In *Finite Elasticity* (edited by D. E. CARLSON and R. T. SHIELD) p. 237. *Martinus Nijhoff*, The Hague.
MARSHALL, I. and THOMPSON, A. B.	1954	*Proc. R. Soc. A***221,** 541.
WARD, I. M.	1971	*Mechanical Properties of Solid Polymers.* Wiley–Interscience, London.

APPENDIX

Certain details of the numerical solution associated with the three-dimensional analysis are briefly discussed here. Three equations of the form (3.18) are to be solved, and this is done iteratively using the Newton–Raphson technique.

At each step of the iterative solution numerical integrations must be performed. To compute the values of g_i defined by (3.19) we use an 8-point Gaussian quadrature formula, while integrations with respect to $\bar{z}$ in (3.18) are calculated with a 17-point Gauss–Hermite quadrature formula. To ensure a uniform accuracy regardless of the sharpness of the transition front, a change of variables $Z = \beta\bar{z}$ is introduced as suggested by the profile shape (3.21). To improve the starting values at the Z_1 station in the Gauss–Hermite scheme, a 5-point Gauss–Laguerre formula is used for the interval $(Z_1, +\infty)$.

With stream functions of the form (3.10) the equation $\bar{r} = \kappa_i \bar{R}$ identifies a streamline for each value of κ_i $(0 \leqslant \kappa_i \leqslant 1)$. We choose 8 values of κ_i such that the corresponding values of $\bar{r}$ coincide precisely with the stations $\bar{r}_i$ used for the Gaussian integrations of (3.19). (These κ_i's are independent of Z!) Our double integration scheme thus results in a grid $(Z_i, \bar{r}_j)$ with $i = 1, \ldots, 22$ and $j = 1, \ldots, 8$ and with $\bar{r}_j$ always lying automatically on the same streamline for a fixed j-value. This simplifies considerably the streamline integrals (4.6) and (4.9) which are evaluated by fixing κ_i and then integrating from one Z_i station to the next. A direct Euler method with a finer mesh (10–20 intervals between consecutive Z_i stations) was used for these integrations.